UCRL-16359 Rev.

cy 3

University of California

Ernest O. Lawrence Radiation Laboratory

SHIELDING ATTENUATION OF NEUTRONS FROM 80-MeV α-PARTICLE BOMBARDMENT OF ELEMENTAL TANTALUM

William W. Wadman III

November 13, 1967

TWO-WEEK LOAN COPY

This is a Library Circulating Copy which may be borrowed for two weeks. For a personal retention copy, call Tech. Info. Division, Ext. 5545

Berkeley, California

UCRL-16359 Rev. cy 2

DISCLAIMER

This document was prepared as an account of work sponsored by the United States Government. While this document is believed to contain correct information, neither the United States Government nor any agency thereof, nor the Regents of the University of California, nor any of their employees, makes any warranty, express or implied, or assumes any legal responsibility for the accuracy, completeness, or usefulness of any information, apparatus, product, or process disclosed, or represents that its use would not infringe privately owned rights. Reference herein to any specific commercial product, process, or service by its trade name, trademark, manufacturer, or otherwise, does not necessarily constitute or imply its endorsement, recommendation, or favoring by the United States Government or any agency thereof, or the Regents of the University of California. The views and opinions of authors expressed herein do not necessarily state or reflect those of the United States Government or any agency thereof or the Regents of the University of California.

Submitted to
Nuclear Science and Engineering

UCRL-16359 Rev.
Preprint

UNIVERSITY OF CALIFORNIA

Lawrence Radiation Laboratory
Berkeley, California

AEC Contract No. W-7405-eng-48

SHIELDING ATTENUATION OF NEUTRONS FROM 80-MeV α-PARTICLE BOMBARDMENT OF ELEMENTAL TANTALUM

William W. Wadman III

November 13, 1967

SHIELDING ATTENUATION OF NEUTRONS FROM 80-MeV α-PARTICLE BOMBARDMENT OF ELEMENTAL TANTALUM*

William W. Wadman III

Lawrence Radiation Laboratory
University of California
Berkeley, California

November 13, 1967

ABSTRACT

The angular distribution, yield, spectra, and attenuation of fast neutrons from the α-particle bombardment of a thick elemental-tantalum target have been simultaneously measured.

Data were obtained by using threshold energy detectors and thermal neutron detectors. Neutron spectra at 0, 60, and 90 deg were calculated with the computer program FLUXPOS. The program uses the activities of the reaction products in the threshold detectors and the reaction cross section as a function of energy to compute the shape and magnitude of the neutron spectrum required to produce the observed activities. Thermal neutron activation foils were placed in the shielding at 6-in. intervals to determine the neutron attenuation profiles at 0, 75, and 90 deg from the target.

Data show that neutron spectral slopes become steeper with increasing angle, and the relaxation lengths (i.e., attenuation thickness expressed in g/cm^2) become less with increasing angle.

A literature search did not reveal any experiments with which these data could be compared.

INTRODUCTION

Simultaneous measurements were made of angular distribution, yield, spectra, and attenuation profiles of fast neutrons. The neutrons were obtained by bombarding a thick elemental tantalum target with 80-MeV α particles accelerated by the Berkeley 88-inch cyclotron. In these experiments we measured the effectiveness of the existing shielding at the cyclotron, and developed data to use in designing local shielding configurations.

The simultaneous measurements of attenuation profiles for three measured incident spectra offer three new sets of data which may assist in refining calculations related to neutron shielding.

A literature search did not reveal previous work with which these experiments could be compared.

METHODS AND APPARATUS

Threshold Detectors

Threshold neutron reaction detectors were used to determine angular distribution, yield, and spectra of the fast neutrons. The choice of materials selected for these detectors was based upon the work of Ringle at this Laboratory (1); the properties, as described in Table I, were taken directly from his work. The neutron spectra calculated from the reaction products of each detector could not incorporate the ^{203}Tl and ^{127}I(n, 2n) reactions. This was due to the lack of accurate experimentally determined neutron reaction cross sections as a function of energy at the time of this data reduction. The neutron spectra were calculated from the γ-ray activities of the reaction products in the detector materials. This was done with an improved version

of Ringle's program FLUX. The improved program, FLUXPOS, was devised by Kohler at this Laboratory (2).

Both Ringle's and Kohler's programs have upper limits of 30 MeV for spectral calculations. Two other reactions were therefore used to extend the spectra beyond 30 MeV; the properties of these two reactions--$^{27}Al(n, \alpha 2n)^{22}Na$ and $^{203}Tl(n, 4n)^{200}Tl$--are also shown in Table I.

Thermal Neutron Detectors

The neutron attenuation profiles were established by using indium foil thermal-neutron detectors (3-5). Indium has a 145-barn thermal-neutron cross section and a half-life of 54.0 minutes, the availability and shape of the foil, and the existing beta-counting system, all contributed toward the decision to use indium for these studies.

Through the use of indium we felt that we could accurately determine the attenuation profiles for concrete, considering processes generally accepted as neutron-attenuating mechanisms (6-9). Concrete is made of elements ranging from medium Z down to hydrogen. Elements in this region of atomic weight perform well as scattering and absorbing materials (6, 7). For those reasons, we felt that by observing the attenuation profiles of the thermal neutrons, we would be indirectly observing the attenuation of the fast-neutron flux.

Further, because of the high thermal-neutron cross section of indium, and the short irradiation time required for saturation activity, we were quite able to obtain significant data with a range of 10^5. With adequate thickness of the shielding and more care in counting low-activity foils, the range could span 10^7. Other experimenters have found a range of 10^4 for foils to be their practical limit (7).

Experimental Setup and Apparatus

Figure 1 is a schematic diagram of the irradiation apparatus and of the beam-alignment and viewing equipment. The aluminum equipment box housed an etched quartz plate oriented at 45 deg to the α-particle beam. Located 90 deg to the beam line and opposite the quartz was a remote, closed-circuit television camera. The extracted α-particle beam was brought out of the cyclotron through a quadrupole focusing magnet and a steering magnet (not shown in Fig. 1) onto the quartz plate, which was placed precisely in the beam line. The beam was centered and shaped while the television readout was being observed. The quartz was then withdrawn, allowing the beam to proceed to the Faraday cup and target.

The Faraday cup was electrically isolated from any ground paths except when it was connected to an integrating beam-current electrometer.

Centered about the target was the threshold-detector mounting ring used to hold the threshold detectors rigid during irradiation.

Detector Mounting

The threshold detectors were first mounted on their support ring 30 cm in diameter. When the beam alignment and tuning were complete, the detectors and ring were mounted on the beam pipe and centered accurately about the target.

The indium detectors were fastened at 6-in. intervals within a flexible tubular hydrocarbon material. The tubing was pressed flat and could be easily placed in slots in the shielding when tuning was complete.

Figure 2 shows the foil locations, spacing, shielding material, and target location for the thermal-neutron-detector experiment.

Target and Mounting

The tantalum target was selected on the basis of the nearly isotropic angular distribution of neutrons, as reported by Allen et al. (10) for 30-MeV α-particle bombardment. Tai et al. (11) showed the neutron yield of tantalum to be high, relative to lower-Z elements, for 32-MeV proton bombardment of thick targets. The results of these works, plus the physical properties--i.e., melting point--were carefully considered in choosing the target material.

The tantalum was machined to fit very closely in the back of the Faraday cup. The target was thus in direct electrical contact with the copper of the cup for accurate beam current indication.

Beam Current Measurements

The beam current of the fully ionized ^{4}He was measured in a Faraday cup of oxygen-free high-conductivity copper. The assembly permitted complete electrical isolation of the cup and vacuum container. The current was measured with an integrating-beam-current electrometer.

To suppress the escape of secondary-emission electrons, a high-voltage guard ring at -1600 V dc preceded the Faraday cup. This ring permitted us to remove the magnet normally used for secondary electron suppression, and thus reduce large masses between the target and detectors. With this type of apparatus, beam-current measurements at this facility were found to be accurate to ± 3% (12).

Beam Alignment and Tuning

Prior to the placement and irradiation of the passive detectors, the beam was centered and shaped while it was bombarding an etched quartz plate (Fig. 1). The quartz luminescence was observed by a remote closed-circuit television camera whose receiver was in the control room. This remote viewing permitted the cyclotron operators to shape and align the beam to ±2 mm. After shaping and alignment, the quartz was withdrawn and the beam was directed onto the target and Faraday cup. The beam current was then maximized on the target.

When the beam current was as high as possible for steady accelerator operation the radio-frequency power was turned off and the detectors were positioned for the experiments.

Counting

Threshold Detectors

Consistent with the technique of neutron spectroscopy developed by Ringle (1), the gamma radiations from the activated threshold detectors were analyzed with a thallium-activated sodium iodide [NaI(Tl)] crystal. The one we used was 3 in. in diam. and 3 in. high, and was mounted in a low-activity matched window assembly.

We counted the samples in a 12-in.-thick serpentine block cave of modest background. (Serpentine is a natural mineral that contains little, if any, radioactivity (13).)

Gamma-ray spectra of the reaction products were accumulated in a 400-channel pulse-height analyzer. The entire spectrometry system was housed in an air-conditioned humidity-controlled atmosphere.

Thermal-Neutron Detectors

The indium foils were counted with a methane gas-flow proportional counter having a 0.6-mg/cm^2 window 1 in. in diameter. The counter was surrounded by a 4-in.-thick lead shield. This counter and associated electronics were housed in an air-conditioned humidity-controlled atmosphere.

All counting electronics were operated from a regulated ac power supply.

DATA REDUCTION AND ANALYSIS

Spectra

The γ-ray spectra of the activated threshold detectors, as measured with the γ-ray spectrometer, were used to calculate the absolute activities of the reaction products. The calculated activities of each type of detector at the same angle were then used in the program FLUXPOS (2) to compute the neutron spectra. The relationships between detector activity, cross section, and neutron flux are expressed as

$$A_i' = \int_0^\infty \phi(E)\, \sigma_i(E)\, dE, \qquad (1)$$

where A' = detector saturation activity or disintegration rate per target nucleus in sec^{-1},

$\phi(E)$ = neutron flux in cm^{-2} sec^{-1} MeV^{-1},

$\sigma(E)$ = reaction cross section in cm^2,

E = neutron energy in MeV,

and i = identification of the reaction and the residual nucleus.

One equation for each threshold reaction was used to form a set of integral equations that described the unknown neutron flux. By

iteration the computer sought to produce a set of calculated activities that best fitted the set of measured activities. When it had such a set, it calculated the neutron flux per energy interval on the basis of the neutron spectrum that would be required to achieve the calculated ratios between (a) the activities and (b) the neutron flux necessary to produce the measured activities.

This technique, which was originated by Ringle (1) and improved upon by Kohler (2), is a Fortran IV program developed at this Laboratory for the IBM 7094. Spectral calculations were printed out as a neutron-flux-per-energy interval (step function) as wide as specified in the data input to the program. (FLUXPOS has been recently written in Fortran 66 for the CDC 6600 computer.)

Angular Distribution of Neutrons

The activities of the threshold detectors, at each angle measured, were used to calculate the total integrated neutron flux required to produce the absolute activity calculated for each reaction product. These numbers gave relative indications of the flux of neutrons with energies greater than the reaction threshold energies. The data from the same reaction, observed at different angles with respect to the target, could be used to describe the angular distribution of neutrons above various threshold energies.

Fast-Neutron Yield

The fast-neutron yield was calculated from the results of the $^{58}Ni(n, p)^{58}Co$ activities and the integrated neutron flux required to produce that yield. The threshold energy of this reaction is 1.1 MeV and can be initiated by any neutron above that energy. The efficiency

of the reaction for all neutrons is a function of the cross section and the energy of the incident neutrons. The neutron emission from the target is not isotropic in the forward direction. The angular distribution from 0 to 60 deg is a diminishing exponential. For larger angles, the angular distribution is apparently constant for the 1.1-MeV reaction.

Based upon the $^{58}Ni(n, p)^{58}Co$ reaction results and flux calculations, the following equation was derived to calculate the total emission of neutrons from the tantalum target:

$$
\begin{aligned}
Q &= \int_0^{\pi} \phi(\theta) 2\pi r^2 \sin\theta \, d\theta \\
&= 2\pi r^2 \int_0^{\pi} \phi(\theta) \sin\theta \, d\theta \\
&= 2\pi r^2 \phi_0 \int_0^{\theta_1} e^{-a\theta} \sin\theta \, d\theta + 2\pi r^2 \phi_k \int_{\theta_1}^{\pi} \sin\theta \, d\theta \qquad (2) \\
&= 2\pi r^2 \phi_0 \times \left[\frac{e^{-a\theta}(-a \sin\theta_1 - \cos\theta_1}{a^2 + 1} \right]_0^{\theta_1} \\
&\quad - 2\pi r^2 \phi_k \cos\theta \Big|_{\theta_1}^{\pi} ,
\end{aligned}
$$

where Q = total neutron emission (neutron sec^{-1} μA^{-1} of alpha particles),

r = 15 cm,

ϕ = neutrons cm^{-2} sec^{-1} μA^{-1},

θ = lab angle (relative to beam angle to target) in radians,

a = 0.9856 for 80-MeV α on Ta,

ϕ_k = flux constant (minimum value of ϕ),

θ_1 = angle beyond which ϕ_k exists ($\approx$60 deg).

Attenuation of Neutrons

The indium foils (thermal-neutron-activation detectors) were used to find the relative thermal-neutron population at each of the measured points in the shielding. In concrete, the relationship between the fast and thermal neutrons is considered to vary proportionally. In iron, a proportional relationship can exist only if the iron is thick enough to produce an equilibrium neutron spectrum. Indium foils may not be used to determine a realistic fast neutron flux attenuation in our iron shielding because in iron fast neutrons undergo inelastic neutron scattering as low in energy as 0.8 MeV. Further energy reduction within the iron is difficult below 0.8 MeV. As the indium foils detect thermal neutrons, the thermal-neutron-induced activities in indium exposed while in a "thin" iron wall may not be used to accurately represent the effectiveness of iron as a fast neutron shielding material for lack of equilibrium spectrum conditions, and an inability to describe reactions and scatter of the fast neutrons.

The indium foils were counted and the activities were corrected for weight, decay time, and saturation activity. The relationship of thermal-neutron activities in indium to fast neutron population within large moderating masses is now under study (14).

EXPERIMENTAL RESULTS

Angular Distributions

The angular distributions of neutrons observed in this experiment are shown in Fig. 3. The curves were drawn through the experimental points which represent the calculated neutron flux at the angles of observation. The data were normalized to a spectrum weighted, average

neutron reaction cross section as a function of energy. The beam current was normalized to a 1-μA beam rate. Each curve represents the angular distribution of neutrons of energies greater than the threshold for that reaction, as given in Table I.

Neutron Spectra

Neutron spectra at 0, 60, and 90 deg from the target were calculated from the threshold detector activities. Figure 4 shows the three spectra calculated with the program FLUXPOS (2) and extended with the higher energy threshold reactions $^{27}Al(2, \alpha 2n)^{22}Na$ and $^{203}Tl(n, 4n)^{200}Tl$.

As the range of FLUXPOS was only from 0.2 to 30 MeV, it was necessary to determine the neutron flux and spectra beyond 30 MeV by means of the data obtained from reactions near to the 30-MeV FLUXPOS cutoff. This was done by using the $^{27}Al(n, \alpha 2n)^{22}Na$ reaction to determine the neutron flux greater than 30 MeV at 0 deg. Because of the sensitivity of this reaction, it became increasingly difficult to use at angles greater than 0 deg because of the sharp decline of high-energy neutrons with increased angle.

A high-energy reaction in thallium was noted and identified by γ-ray energy and half-life. The reaction threshold was calculated with the mass-difference formula, and the threshold reaction energy was compared with some experimental data.

The calculated value of 24.7 MeV was close to the energy necessary to initiate a $^{203}Tl(\gamma, 3n)^{200}Tl$ reaction, as experimentally determined by Moffatt and Reitmann (15).

The ^{22}Na activity at 0 deg was compared with the ^{200}Tl activity at 0 deg, and as the two reactions have similar threshold energies and reaction cross-section shapes, we therefore assumed that the neutron flux responsible for the ^{22}Na activity was identical to that which produced the ^{200}Tl activity. The ^{200}Tl activities at the other angles of observation were compared with the ^{200}Tl and ^{22}Na activities at 0 deg to derive the total neutron flux of 30 MeV or greater energy.

The neutron spectra, calculated by FLUXPOS as high as 30 MeV, had slopes of $E^{-1.7}$ at 0 deg, $E^{-2.3}$ at 60 deg, and $E^{-3.2}$ at 90 deg, in the energy region from 6 to 30 MeV. When a thick, high-Z target was bombarded by α particles, we did not expect to observe a peak in the high-energy portion of the neutron spectrum. Therefore we assumed that the spectral shapes would maintain their respective slopes out to the cutoff energies (16, 17). The neutron flux greater than 30 MeV for each angle was then distributed according to the slope until the total flux at each angle was accounted for.

The general spectral shapes are similar to the neutron spectra at various angles as calculated by Moyer (17). His spectra, for protons on beryllium, have a broad peak at the high-energy region in the forward angles. This would be expected in a single-nucleon bombardment of a low-Z target (17).

Fast-Neutron Yield

The fast-neutron yield (emission) was calculated by means of Eq. 1. The "Q" (emission) was evaluated at 3.0×10^{11} neutrons sec^{-1} μA^{-1} of α particles. Activities of the ^{58}Ni(n, p)^{58}Co threshold reaction were used to determine the angular distribution of the neutron flux.

By use of that information, the angular flux was integrated and corrected to 4π geometry for the neutron emission rate.

Some neutron production by α-particle bombardment has been studied. 30-MeV α particles on tantalum were studied by Allen et al. (10), who used the $^{32}S(n, p)^{32}P$ threshold reaction. The values obtained from their work were based upon straight-line extrapolations that they made for tantalum targets. Their value, of about 9.8×10^7 neutrons sec^{-1} μA α $particles^{-1}$, is considerably low by our measurements and estimates. Assuming that our spectra are reasonable, one finds a large number of neutrons in the regions 0.2 to 4 and 4 to 8 MeV. Comparing the $^{32}S(n, p)^{32}P$ reaction threshold with the $^{58}Ni(n, p)^{58}Co$ reaction threshold, one could find an immediate 25% difference. Accounting for the very significant difference in the incident energies, one might find an even larger difference between measured and calculated fast-neutron emission rate.

The ratios of neutron emission rates at 50- and 100-MeV α-particle energies were studied by the author. The emission ratios at α-particle energies of 50 to 100 MeV are plotted along with Allen's data (10) at 30 MeV, a 40-MeV emission value determined by the author (18), and the 80-MeV emission value presented here, in Fig. 5.

Total neutron yield from thin targets for 40-MeV α bombardments are in reasonable agreement with data presented here when some attempt is made to account for the difference in the thickness of the targets (19).

Neutron-Attenuation Profiles

Activities produced by forward-directed neutrons were corrected for angular distribution to derive attenuation profiles for 0° neutrons. This was necessary because only perpendicular slots in the wall were available in which to insert the indium foils, whereas the beam angle was 15 deg from a perpendicular with the shielding wall. The 75-deg and 90-deg profiles were from straight-line irradiations, so that only inverse-square corrections were made in determining the attenuation profile.

Figure 6 shows the attenuation profiles for the three different angles. The data, corrected for $1/R^2$ from the target, were plotted against the thickness of the shielding.

The 1/e attenuation lengths (relaxation lengths in g/cm^2) of the shielding materials, determined with thermal neutron detectors, are given in Table II.

Neutron attenuation in ordinary concrete has been measured at several laboratories (8, 9, 17). By applying our measured relaxation lengths to the experimentally determined attenuation values for mono-energetic neutrons, we can infer effective neutron energies. These values are contained in Table II.

Although data for the attenuation lengths in iron are given, we feel that they should be considered with the following reservations:

a. Thermal neutron detectors were used to collect the data; and thermal-neutron detectors may not adequately describe the fast-neutron attenuation in iron, except where the iron is thick enough to permit spectral equilibrium.

b. Iron is a poor moderator; and although neutrons undergo inelastic scattering down to about 0.8 MeV, they lose little energy below this value.

It is interesting to note the straight-line attenuation curve in the iron at 75 deg (Fig. 6). (One explanation is the proximity of concrete on the other side of a 3-in. iron slab attached to the concrete wall.) Experimental results in iron for spectra with energies between those measured at 0 deg and 75 deg would help to shed light on the effects of iron on neutrons of energies between 30 and 60 MeV.

CONCLUSIONS

The angular distribution, yield, spectra, and attenuation profiles of neutrons have been measured simultaneously. The experiments were performed while elemental tantalum was being bombarded with 80-MeV α particles. The work was done with techniques described in the literature.

The angular distribution of neutrons was measured with several types of threshold detectors. The high energy neutron component is easily observed as higher energy threshold reactions are used, especially in the forward direction.

The fast neutron yield of the experiment was calculated from the $^{58}Ni(n, p)^{58}Co$ reaction, corrected for anisotropy, and was evaluated at 3.0×10^{11} neutrons sec^{-1} μA^{-1}. This value is accurate to $\pm 25\%$.

The neutron spectra were calculated with an IBM 7094 computer, which, by iteration, produced a set of calculated activities which agreed best with the measured activities. It then calculated the flux and spectrum required to produce the measured activities.

The fast neutron attenuation profiles were derived by using thermal neutron detectors inserted in slots in the shielding materials. The 1/e attenuation values, expressed in g/cm^2, are 48 at 0 deg, 29 at 75 deg, and 32 at 90 deg in concrete; and 147 at 0 deg and 92 at 75 deg in iron. The relaxation lengths in concrete at 0 and 75 deg were obtained after the neutrons had first penetrated the iron part of the wall.

The values expressed are considered to be accurate if the thermal neutron detector results adequately represent the attenuation of the incident neutron spectra.

ACKNOWLEDGMENTS

I thank the members of the Health Physics Department for their constant encouragement and assistance.

FOOTNOTES AND REFERENCES

*Work done under auspices of the U. S. Atomic Energy Commission.

1. John Clayton Ringle, Techniques for Measuring High-Energy Neutron Spectra Using Threshold Detectors (Ph. D. Thesis), Lawrence Radiation Laboratory Report UCRL-10732, Oct. 1963 (unpublished).
2. Arthur D. Kohler, Jr., An Improved Method of Neutron Spectroscopy Using Threshold Detectors (M. S. Thesis), Lawrence Radiation Laboratory Report UCRL-11760, Dec. 1964 (unpublished).
3. Lloyd D. Stephens and Alan R. Smith, Fast Neutron Surveys Using Indium Foil Activation, Lawrence Radiation Laboratory Report UCRL-8418, Aug. 1958 (unpublished).
4. William W. Wadman III, Neutron Shielding Attenuation Profiles of the 88-Inch Cyclotron, Lawrence Radiation Laboratory Report UCID-2434, Aug. 1963 (unpublished).
5. William W. Wadman III, Summary of Shielding Calculations Based on the Texas A & M University 88-Inch Cyclotron Specifications, Lawrence Radiation Laboratory Report UCID-2437, Dec. 1964 (unpublished).
6. J. Greenborg, Neutron Attenuation Mechanisms in Concrete, for the American Society for Testing and Materials, June 1965.
7. E. Aalto and R. Nilsson, Attenuation in Massive Laminated Shields of Concrete and a Study of the Accuracy of Some Methods of Calculation, Aktiebolaget Atomenergi Report AE-157, 1964.
8. Roger Wallace, Cyclotron Shielding, Lawrence Radiation Laboratory Report UCRL-11315, Aug. 1965.

9. H. Wade Patterson, Accelerator Radiation Monitoring and Shielding, Lawrence Radiation Laboratory Report UCRL-16445 Rev., Nov. 1965 (unpublished); H. Wade Patterson, The Effects of Shielding on Radiation Produced by the 730-MeV Synchrocyclotron and the 6.3-BeV Proton Synchrotron at the Lawrence Radiation Laboratory, in Proceedings of the First International Conference of Shielding Around High-Energy Accelerators (Presses Universitaires de France, Paris, France, 1962).

10. A. J. Allen, J. F. Nechaj, K. H. Sun, and B. Jennings, Phys. Rev. 81, 536 (1951).

11. Yuin-Kwei Tai, George P. Millburn, Selig N. Kaplan, and Burton J. Moyer, Phys. Rev. 109, 2086 (1958).

12. John R. Meriwether (Lawrence Radiation Laboratory), private communication, 1964.

13. Harold A. Wollenberg and Alan R. Smith, Earth Materials for Low-Background Radiation Shielding, Lawrence Radiation Laboratory Report UCRL-9970, May 1962 (unpublished).

14. Alan R. Smith and Alvin J. Miller (Lawrence Radiation Laboratory), private communication, 1965.

15. J. Moffatt and D. Reitmann, Nucl. Phys. 65, 130 (1965).

16. H. Wade Patterson, Roger W. Wallace, and Alan R. Smith (Lawrence Radiation Laboratory), private communication, 1965.

17. Burton J. Moyer, Shielding and Radiation Calculations for the USNRDL Cyclotron, Lawrence Radiation Laboratory (unpublished report compiled in 1960).

18. William W. Wadman III, Health Phys. 11, 659 (1965).

19. Edward L. Hubbard, Robert M. Main, and Robert V. Pyle, Phys. Rev. 118, 507 (1960).

Table I. Threshold detector properties (from Ref. 1).

Reaction	Calculated threshold (MeV)[a]	Peak cross section (barns)	Product half-life	Target isotope (%)	γ-Ray energy of product (MeV)
$^{58}Ni(n, p)^{58}Co$	1.1	0.556	71 days	67.8	0.81
$^{59}Co(n, \alpha)^{56}Mn$	5.4	0.112	2.6 hr	100	0.845
$^{65}Cu(n, p)^{65}Ni$	4.1	0.035	2.6 hr	30.9	1.5
$^{27}Al(n, \alpha)^{24}Na$	6.7	0.243	15 hr	100	1.37
$^{203}Tl(n, 2n)^{202}Tl$	8.5	2.78	12 days	29.5	0.44
$^{127}I(n, 2n)^{126}I$	9.5	2.02	13 days	100	0.65
$^{58}Ni(n, 2n)^{57}Ni$	12.4	0.25	37 hr	67.8	1.36
$^{27}Al(n, \alpha 2n)^{22}Na$	23.4	0.030	2.6 yr	100	0.51, 1.27
$^{203}Tl(n, 4n)^{200}Tl$	24.7	≈1.3	27 hr	29.5	1.207

a. The energy at which the cross section value is 2% of the maximum cross section value.

Table II. Neutron relaxation lengths in 88-inch cyclotron shielding from 80-MeV α's on tantalum.

Location	Angle (deg)	Relaxation lengths (g/cm^2)		Shielding configuration	Effective neutron energy (MeV)
		In iron	In concrete		
Forward wall	0	147	48	2.5-ft Fe followed by 5.0 ft concrete	40
West door	75	92	29	2.2-ft Fe followed by 2.3 ft concrete	17
Roof	90	-	32	6.6 ft concrete	19

FIGURE CAPTIONS

Fig. 1. Preirradiation alignment apparatus and experimental setup for measurements with threshold detectors.

Fig. 2. Experimental setup for neutron-attenuation-profile measurements made with indium foils.

Fig. 3. Angular distribution of neutrons for five threshold energy levels.

Fig. 4. Neutron spectra for 0, 60, and 90 deg with the 0.2- to 30-MeV regions calculated by program FLUXPOS, and 30 MeV to cutoff regions calculated from the ^{22}Na and ^{200}Tl activities.

Fig. 5. Neutron production by α particles on tantalum as a function of incident particle energy (30-MeV data from Ref. 10, 40-MeV data from Ref. 18, other energies from Ref. 18).

Fig. 6. Neutron attenuation profiles at 0, 75, and 90 deg for neutrons from 80-MeV α particles on a thick tantalum target.

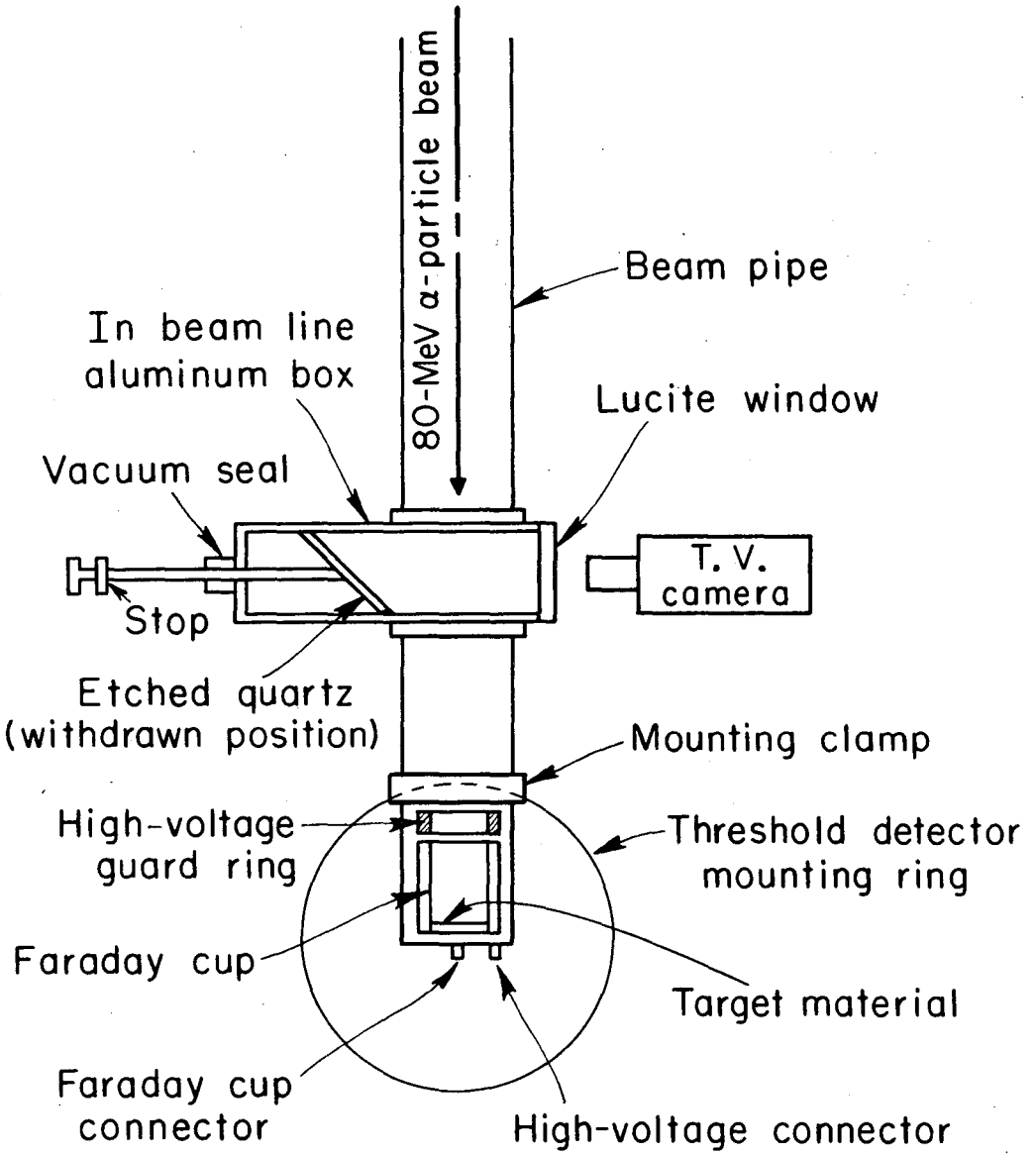

MUB-8267

Fig. 1

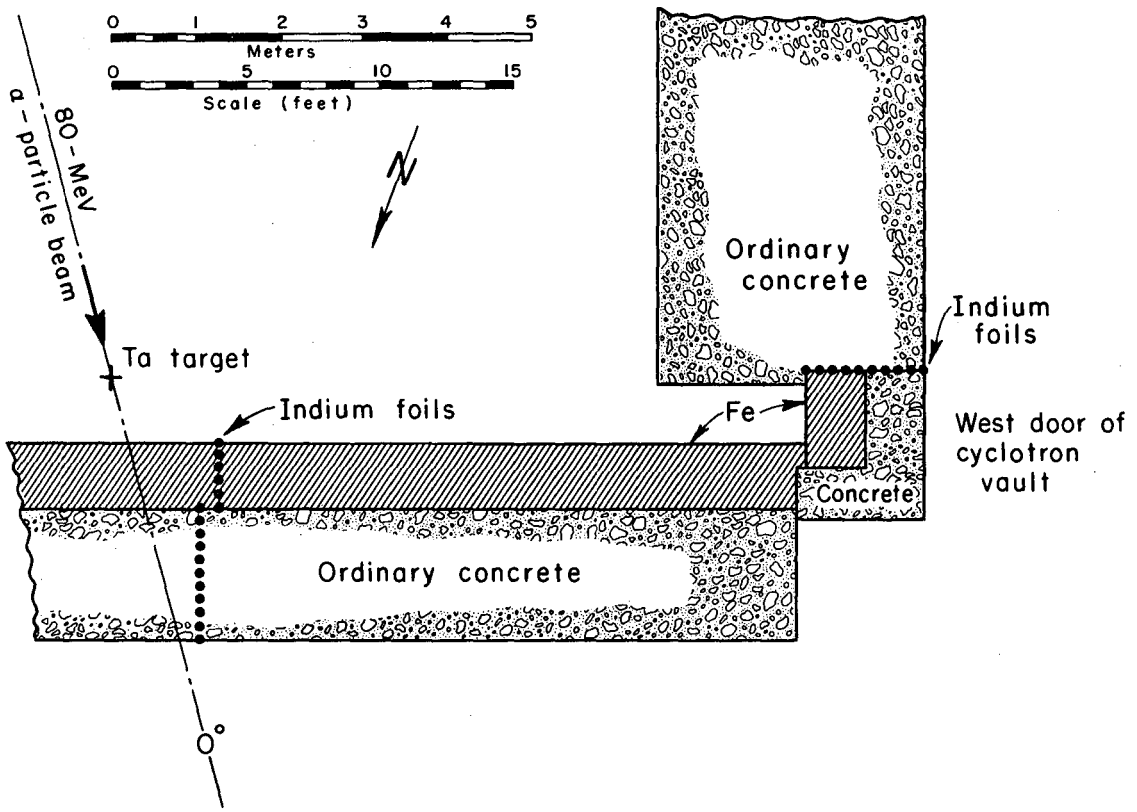

MUB-9537

Fig. 2

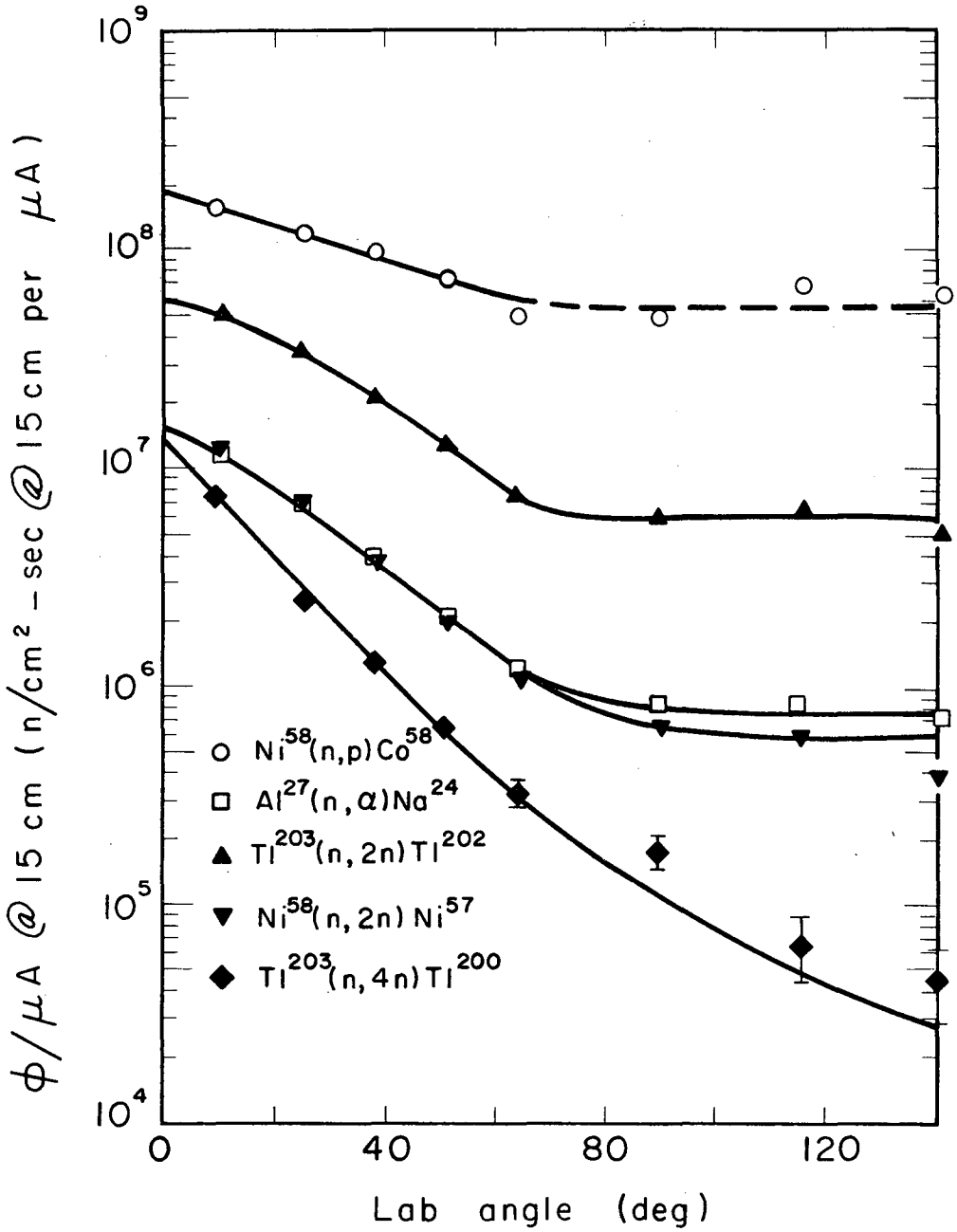

MUB-8264

Fig. 3

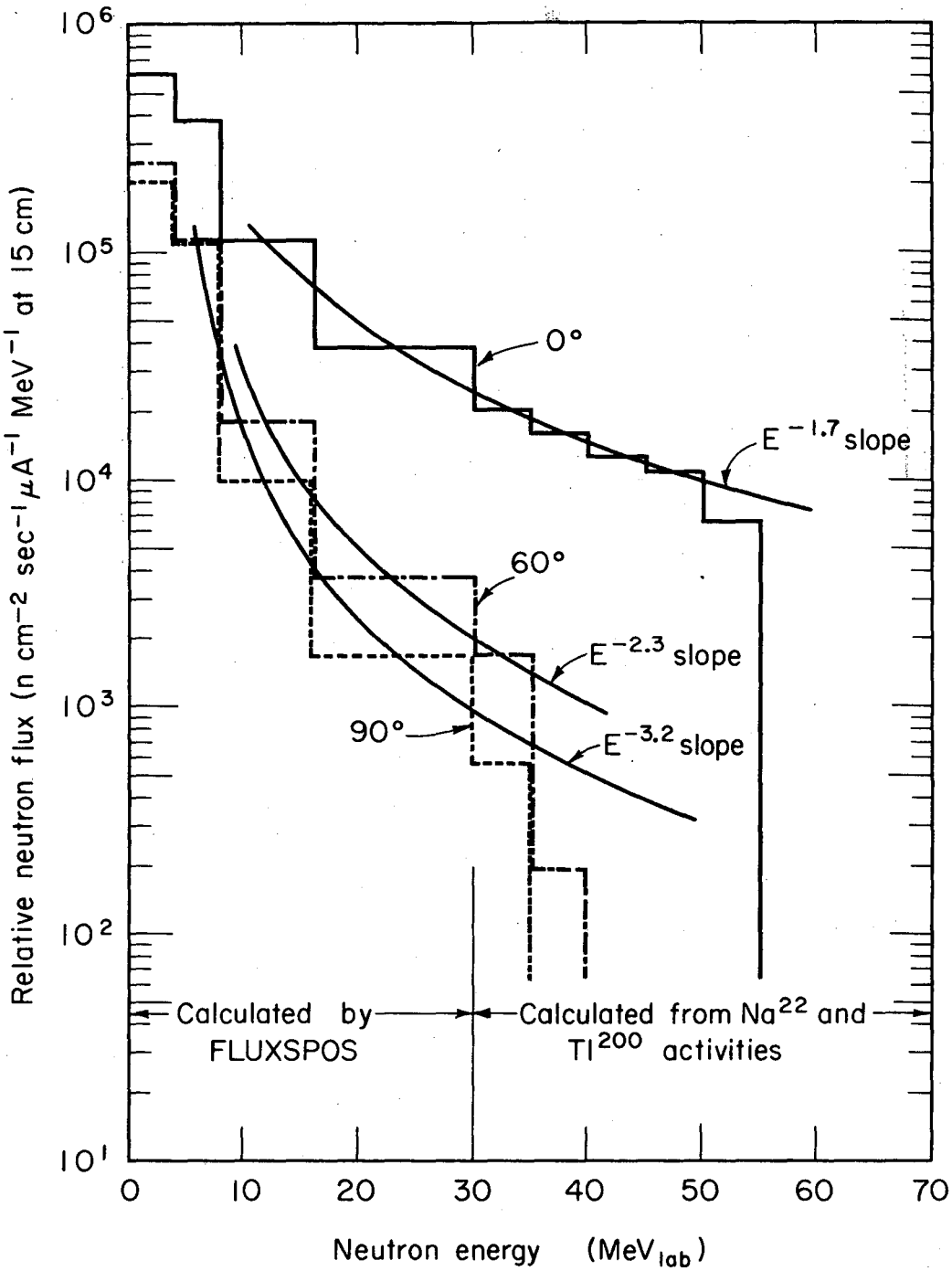

MUB-11022

Fig. 4

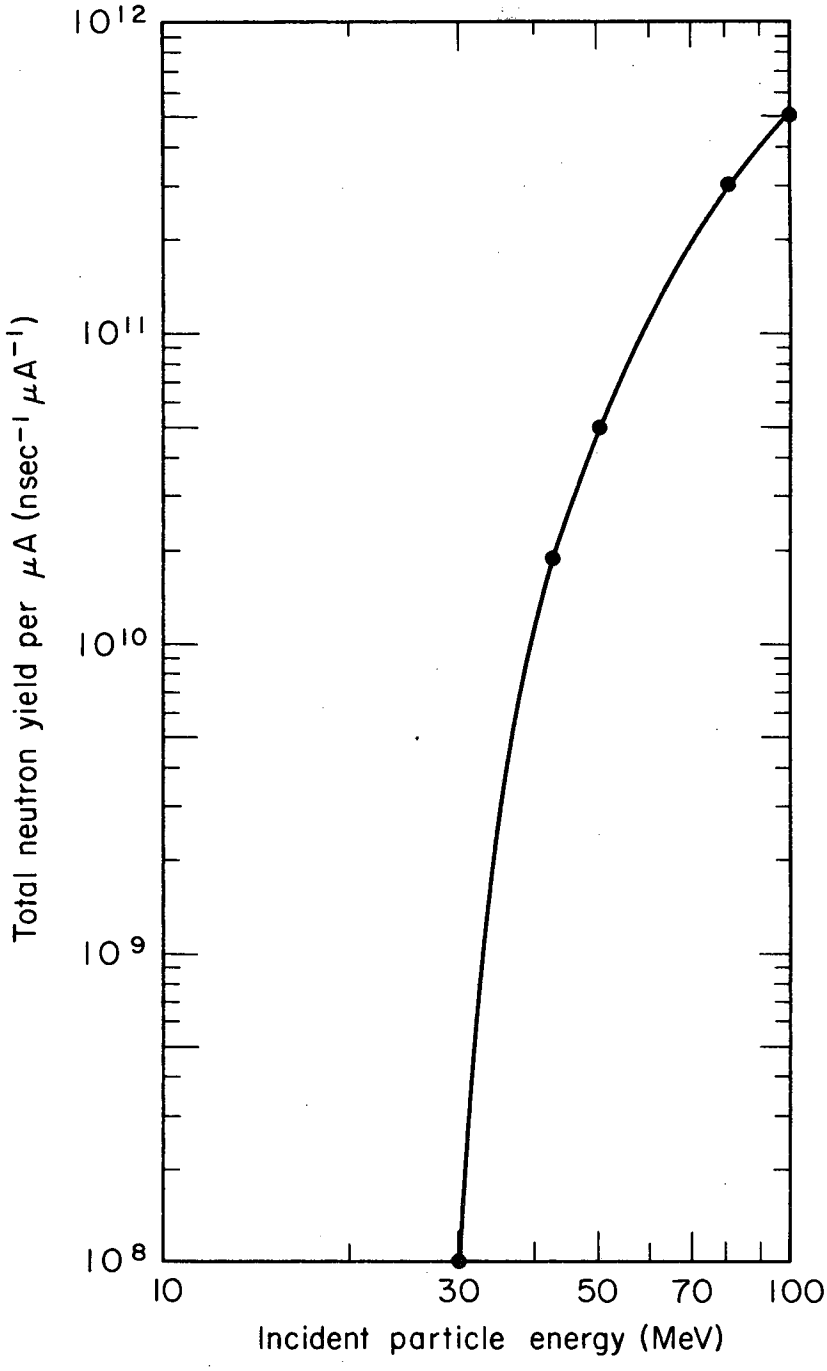

MUB-11023

Fig. 5

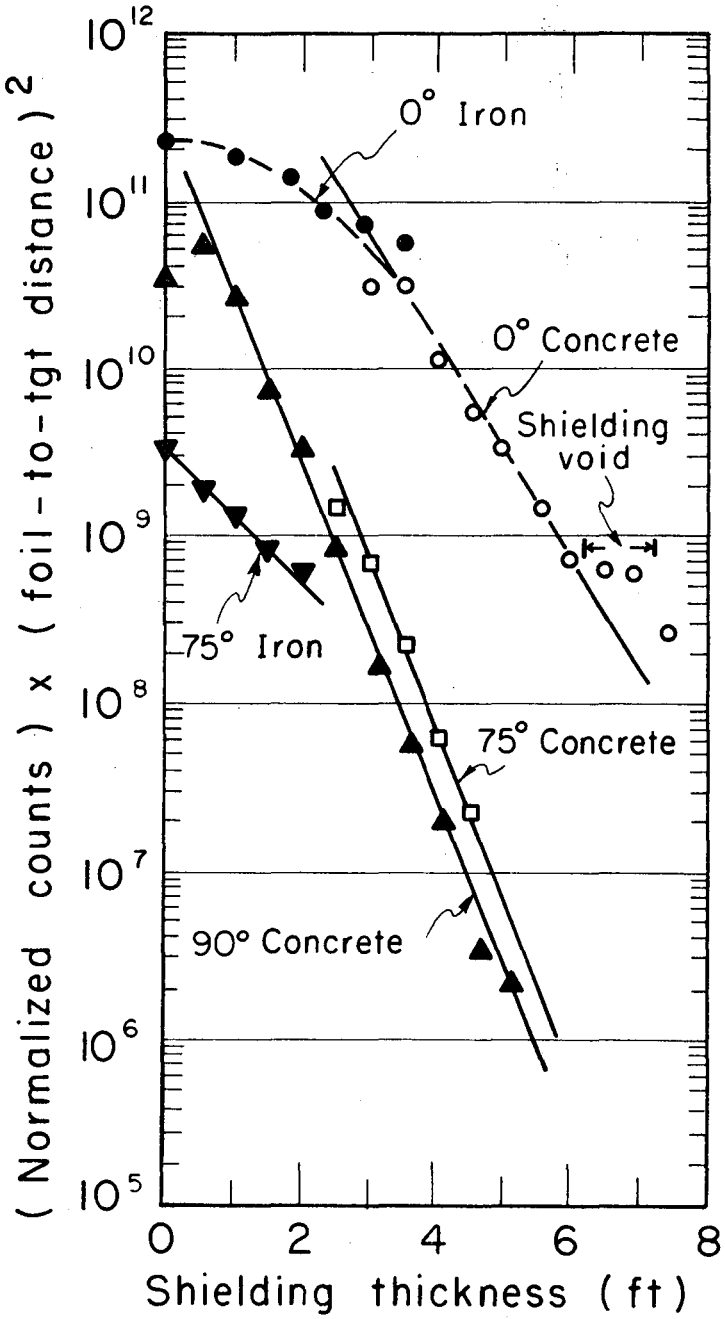

MUB-8262

Fig. 6

This report was prepared as an account of Government sponsored work. Neither the United States, nor the Commission, nor any person acting on behalf of the Commission:

A. Makes any warranty or representation, expressed or implied, with respect to the accuracy, completeness, or usefulness of the information contained in this report, or that the use of any information, apparatus, method, or process disclosed in this report may not infringe privately owned rights; or

B. Assumes any liabilities with respect to the use of, or for damages resulting from the use of any information, apparatus, method, or process disclosed in this report.

As used in the above, "person acting on behalf of the Commission" includes any employee or contractor of the Commission, or employee of such contractor, to the extent that such employee or contractor of the Commission, or employee of such contractor prepares, disseminates, or provides access to, any information pursuant to his employment or contract with the Commission, or his employment with such contractor.